

Research Article

Finite Element Analysis of the Dynamics of Power-Law Fluid around an Obstacle in a Channel

Rashid Mahmood ¹, Mohammed M. M. Jaradat ², Rifaqat Ali ³, Imran Siddique ⁴,
Afraz Hussain Majeed ¹ and Asif Mehmood¹

¹Department of Mathematics, Air University, PAF Complex E-9, Islamabad 44000, Pakistan

²Mathematics Program, Department of Mathematics, Statistics and Physics, College of Arts and Sciences, Qatar University, Doha 2713, Qatar

³Department of Mathematics, College of Science and Arts, King Khalid University, Muhayil, Abha 61413, Saudi Arabia

⁴Department of Mathematics, University of Management and Technology, Lahore-54770, Pakistan

Correspondence should be addressed to Mohammed M. M. Jaradat; mmjst4@qu.edu.qa and Imran Siddique; imransmsrazi@gmail.com

Received 20 January 2022; Accepted 5 April 2022; Published 27 April 2022

Academic Editor: Jiafu Su

Copyright © 2022 Rashid Mahmood et al. This is an open access article distributed under the Creative Commons Attribution License, which permits unrestricted use, distribution, and reproduction in any medium, provided the original work is properly cited.

Control of fluid forces is an emerging area of research with numerous engineering applications. The uneven wake behind an obstacle causes undesirable structural oscillations, which can lead to fatigue or structural failure. Controlling the wake phenomena could directly benefit a wide range of engineering applications, including skyscrapers, naval risers, bridges, columns, and a few sections of airplanes. This study is concerned with the time dependent simulations in a channel in presence of an obstacle aiming to compute fluid forces. The underlying mathematical model is based on nonstationary Navier–Stokes equations coupled with the constitutive relations of power law fluids. Because the representative equations are complex, an effective computing strategy based on the finite element approach is used. To achieve higher accuracy, a hybrid computational grid at a very fine level is used. The $\mathbb{P}_2 - \mathbb{P}_1$ elements based on the shape functions of the second and first-order polynomials were used to approximate the solution. The discrete nonlinear system arising from this discretization is linearized by Newton's method and then solved through a direct linear solver PARADISO. The code validation study is also performed for Newtonian fluids as a special case, and then the study is extended to compute drag and lift forces for other cases of viscosity as described by the power law index. When looking at the phase plot, it can be seen that for the Newtonian case $n = 1$, there is only one closed orbit after the steady state is reached, whereas for $n = 0.5$, there are multiple periodic orbits. Moreover, the effects of shear rate on the drag-lift phase plot are also discussed.

1. Introduction

The significance of flow around bluff bodies has been realized since the last couple of centuries, and hence it is considered as benchmark problem in fluid dynamics. Hence, researchers investigated different shapes of bluff bodies submerged in different fluids for their analysis. It has been proved both experimentally and analytically that hydrodynamic forces like drag and lift around obstacles play an important role in designing structures in many engineering applications. It is also worthy to mention that the interaction of fluid flow with such bluff bodies produces wake, and the

formation of wake around these complex geometries is germane to understand due to its practical utilization. Some investigations are available in recent literature that realize the importance of such configurations in theoretical as well as practical aspects. Hussain et al. [1] considered a circular cylinder to investigate the incompressible flow behavior. The nonlinear fluid for specific values of n is used by Chhabra et al. [2] to investigate the blockage ratios. In [3], shear thinning and shear thickening behavior are observed for the range $100 \leq Re \leq 500$. Drag and lift for a circular cylinder placed in a channel are studied in [4]. Lid-driven flow behavior is observed in [5]. A comparison of drag and lift for

circular and square cylinders can be seen in [6]. Williamson [7] summarized some of the work about this benchmark. The results proposed by Schäfer et al. [8] consider Newtonian fluid at various Reynolds numbers for hydrodynamic forces. They justified the credibility of their work by constructing a comparison with experimental data and also using different computational approaches for attaining the solution. Fluid past a rotating and stationary cylinder is considered in [9, 10] to perform the numerical simulations. They computed instantaneous streamlines along with drag and lift. At low Reynolds number ($0 \leq Re \leq 50$), Tritton [11] performed analysis on the interaction of fluid flow with a circular obstacle and measured hydrodynamic forces. To demarcate the flow regime, Coelho and Pinho [12] used shear thinning fluids for elucidating the vortex shedding. Gupta et al. [13] investigated the steady flow features in Newtonian fluid for Reynolds number ($5 \leq Re \leq 40$). For sake of brevity, some more investigations across circular cylindrical obstacles are referred to in [14–18]. In [14], Bharti et al. presented a numerical study of heat transfer using the finite volume method. Some aspects of flow behavior around a circular cylinder are presented in [15]. The 2D and 3D computational analysis of fluid flow around a cylinder is discussed in [16]. Rajani et al. [17] used different values of Reynolds number to observe the impact of flow behavior around a circular cylinder. Very slow flow around a cylinder is numerically investigated in [18].

A lot of numerical work has been accomplished to explore drag and lift forces on obstacles in the Newtonian flow field, but for non-Newtonian cases, the investigations are still at an embryonic stage to assess the relationship between drag and lift, especially for highly nonlinear viscosity. For nonlinear viscosity fluids, the flow around cylinders of different shapes is an interesting topic of research due to the investigation of the wake, recirculation zone length, and drag and lift characteristics. To analyse the laminar flow of non-Newtonian fluid around a circular cylinder, Chhabra et al. [2] used three values of Reynolds (1, 20, and 40). They used a finite difference scheme to observe the flow pattern. Mossaz et al. [19] used the most generic Herschel–Bulkley fluid model to evaluate the flow pattern around a circular cylinder. In [20], Nejat et al. used power law fluid for their numerical investigations. With the help of the Lattice Boltzman method, they computed drag and lift coefficients. In the low Reynolds number range ($5 \leq Re \leq 40$), the relationship between n and drag coefficient is investigated in [21]. Whitney and Rodin [22] proposed some results for shear thinning fluids. These results are compatible with some previous studies of flow around bluff bodies. The power law fluid past a heated cylinder is used in [23] to observe heat transfer characteristics. In order to eliminate the impact inlet and outlet on the results, some researchers [24–26] used very large computational domains to reduce such effects. The results show that for a circular cylinder, drag is inversely proportional to the computational grid. Abegunrin et al. [27] investigated a non-Newtonian fluid simulation on the upper horizontal surface of a paraboloid of revolution. It is deduced that when the flow is described as Newtonian fluid flow, the maximum velocity of the flow can be determined.

Similarly, Patnana et al. [10] considered unsteady power-law (PL) fluid past a circular cylinder and calculated some results using the finite volume method.

In the literature, there is only a small contribution towards non-Newtonian fluids moving around obstacles and the computation of fluid forces. There is a need to see the impact of shear-thinning and thickening behavior on drag and lift forces. The aim of this article is to elucidate the characteristics of unsteady nonlinear fluid flow in a channel over a cylinder and the estimation of fluid forces. The present work is organized as follows: a limited survey highlighting the importance of flow configuration is presented in Section 1. In Section 2, the adopted research methodology is discussed with details of all solvers. The simulation results and analysis through graphs and phase-plots are performed in Section 3. The present attempt is concluded in Section 4.

2. Research Methodology

2.1. Mathematical Formulation. The mathematical model for an incompressible, isothermal, and nonlinear viscosity fluid model is given by the following set of nonlinear equations, as shown in [30]:

$$\frac{\partial u_i}{\partial x_i} = 0, \quad (1)$$

$$\begin{aligned} \frac{\partial u_i}{\partial t} + \frac{\partial}{\partial x_j} (u_i u_j) + \frac{1}{\rho} \frac{\partial p}{\partial x_i} \\ = \frac{1}{\rho} \frac{\partial}{\partial x_j} \left[\mu(\dot{\gamma}) \left(\frac{\partial u_i}{\partial x_j} + \frac{\partial u_j}{\partial x_i} \right) \right], \quad i, j = 1 \dots 3, \end{aligned} \quad (2)$$

we couple equations (1) and (2) with the well-known power-law model as

$$\mu(\dot{\gamma}) = m(\dot{\gamma})^{n-1}, \quad (3)$$

where m represents the coefficient of fluid consistency; n is the power law exponent.

2.2. Problem Description and Numerical Approach. The computational domain is a channel $\Omega = [0, 2.2] \times [0, 0.41]$, as considered in [28–30]. The circular obstacle is placed at (0.2, 0.2) that is offset from the center to generate a nonzero lift. The top and bottom walls offer no slip conditions as $u = v = 0$. An inflow parabolic profile with maximum velocity as $U_{\max} = 1.5$ is exposed at the inlet of the channel to produce a periodic flow regime and a zero Neumann condition at the outlet. More elements are considered around the obstacle to accurately capture the hydrodynamic forces on the cylinder.

The coarse grid for present simulations is shown in Figure 1. To achieve higher accuracy, one element is mapped into four dotted elements of smaller size by joining the midpoints of the sides of the parent element through h-refinement. Following this strategy of refinement, Table 1 shows the details about the cardinality of elements and degrees of freedom (DOF) at various computational refinement levels.

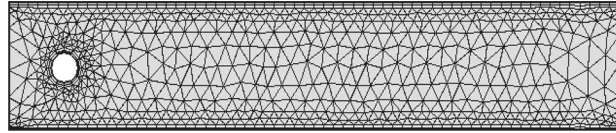


FIGURE 1: Computational grid at level-1.

TABLE 1: Grid statistics at various levels.

Levels	# Elements	#DOF
1	962	7378
2	1590	12009
3	2426	17918
4	4540	32683
5	6716	47611
6	11796	81603
7	27194	187374
8	65288	444873

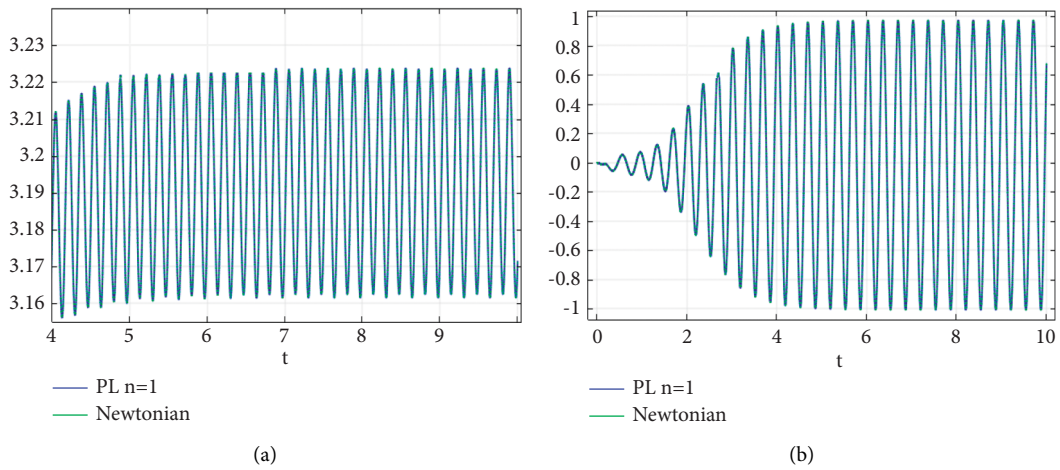


FIGURE 2: C_D and C_L values at $n = 1.0$. (a) C_D . (b) C_L .

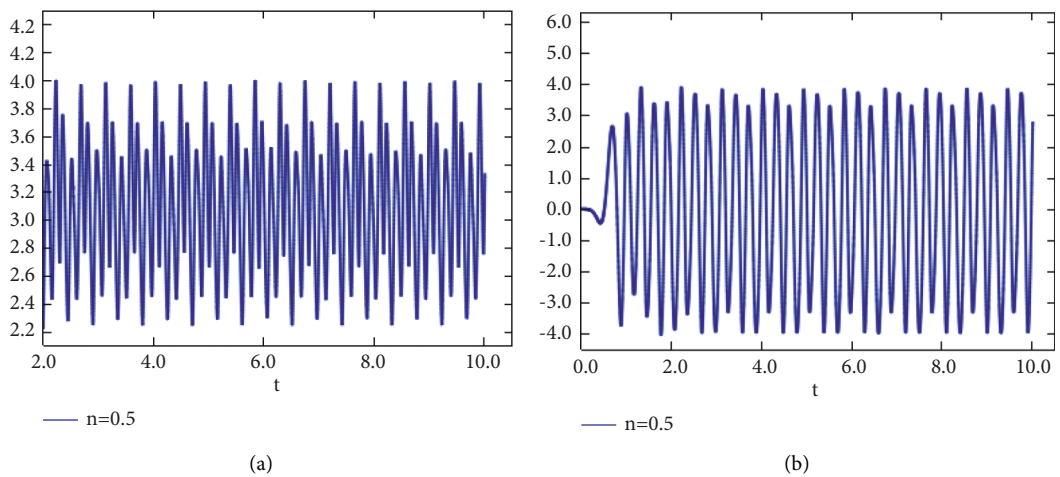


FIGURE 3: C_D and C_L values at $n = 0.5$. (a) C_D . (b) C_L .

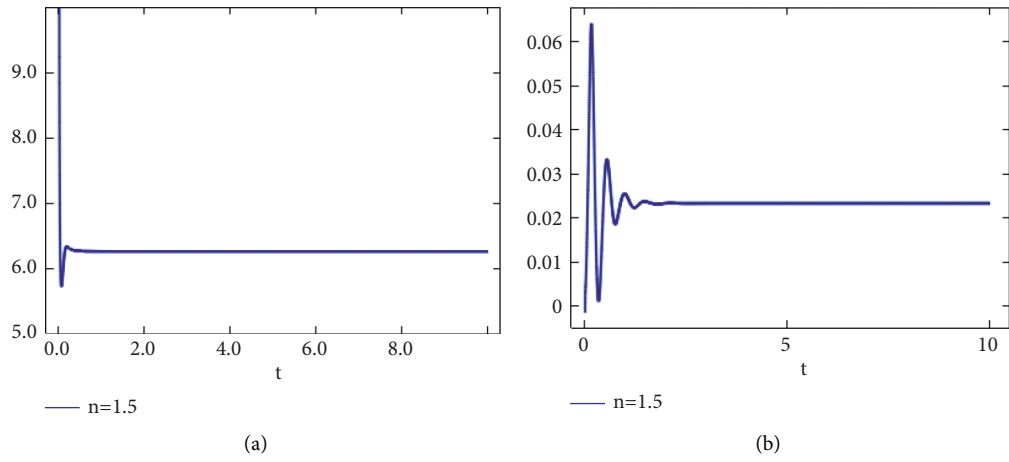


FIGURE 4: C_D and C_L values at $n = 1.5$. (a) C_D . (b) C_L .

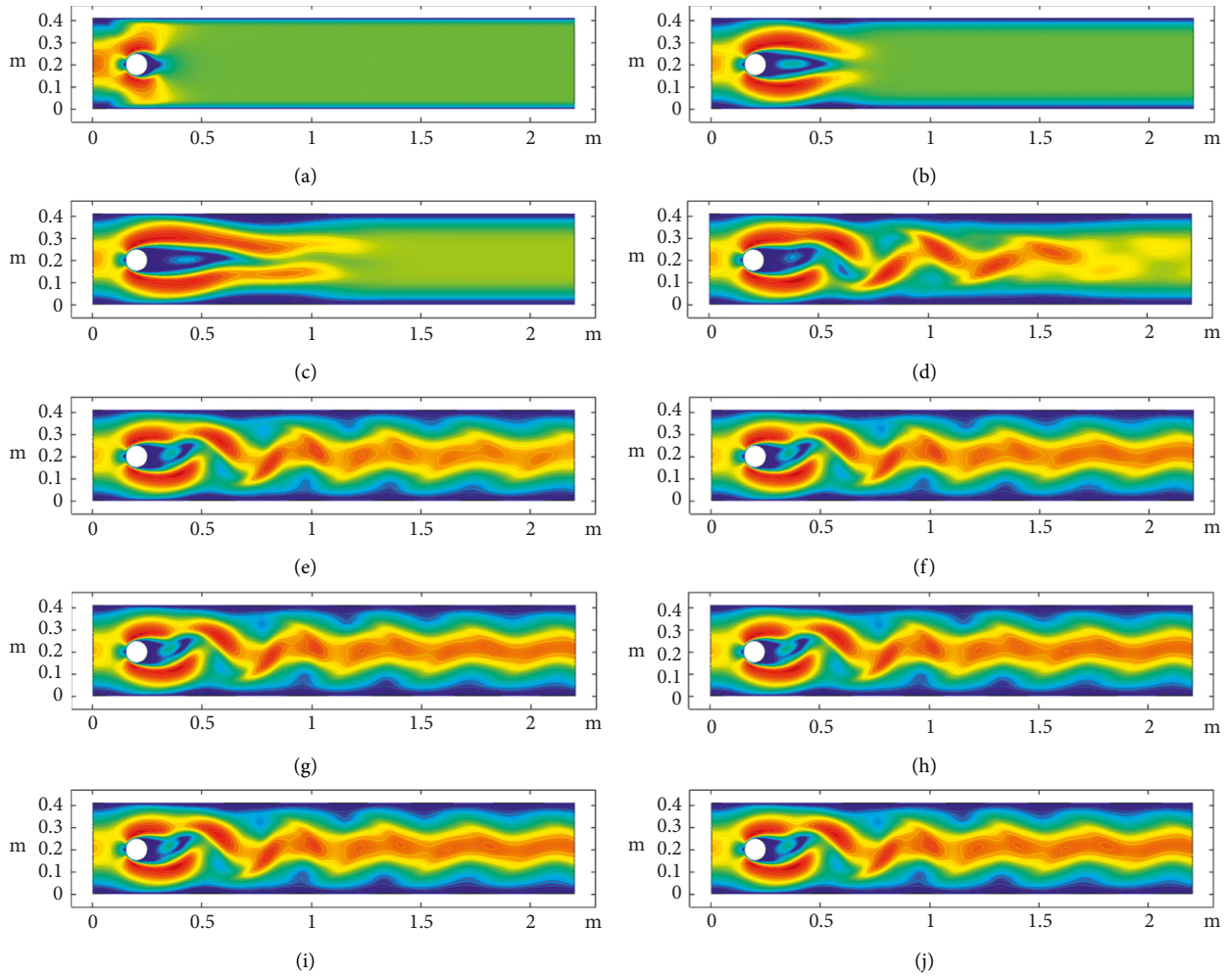


FIGURE 5: Velocity profiles for $n = 1.0$ at various values of time. (a) $t = 0.1$. (b) $t = 0.5$. (c) $t = 1$. (d) $t = 2$. (e) $t = 3$. (f) $t = 4$. (g) $t = 5$. (h) $t = 6$. (i) $t = 7$. (j) $t = 8$.

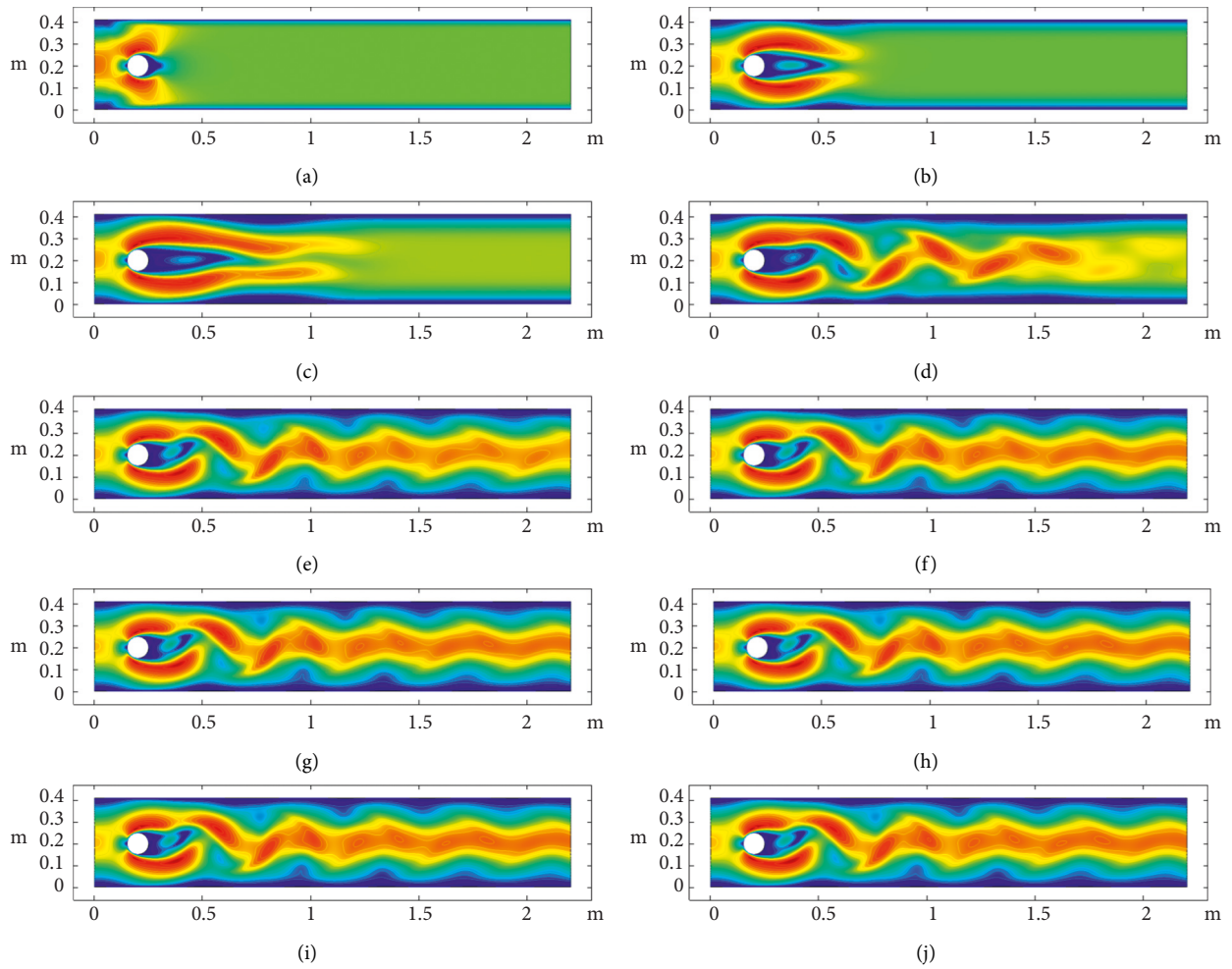


FIGURE 6: Velocity profiles for $n = 0.5$ at various values of time. (a) $t = 0.1$. (b) $t = 0.5$. (c) $t = 1$. (d) $t = 2$. (e) $t = 3$. (f) $t = 4$. (g) $t = 5$. (h) $t = 6$. (i) $t = 7$. (j) $t = 8$.

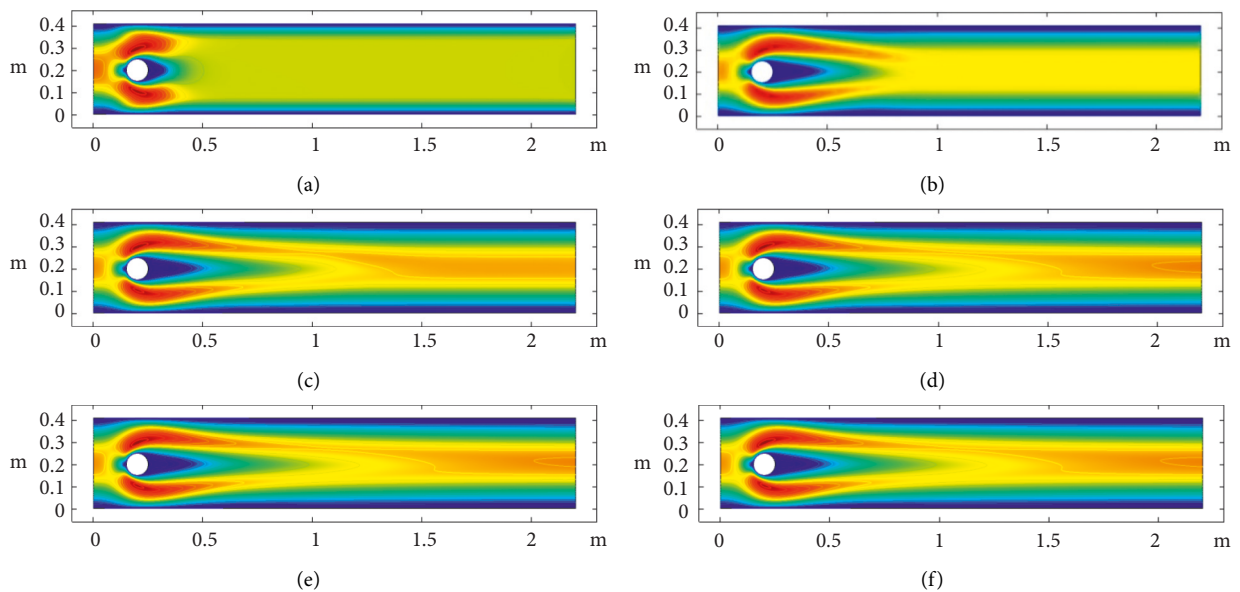


FIGURE 7: Continued.

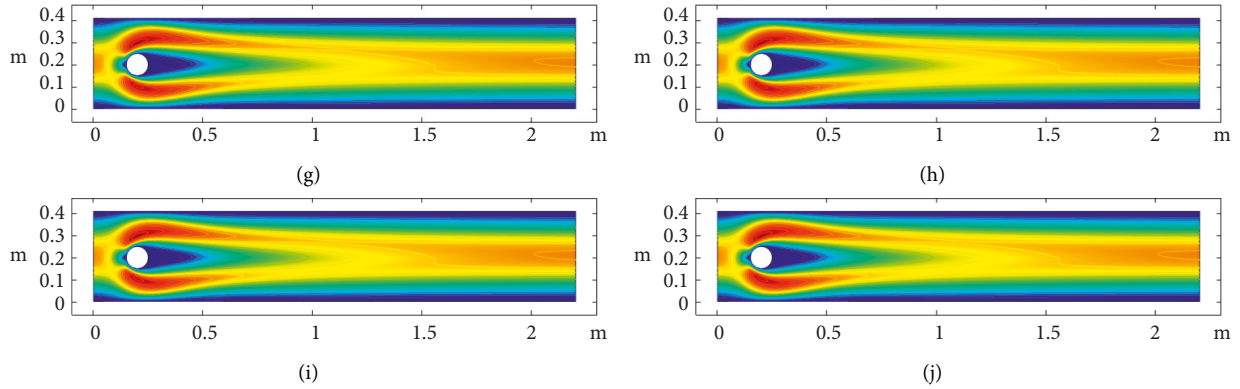


FIGURE 7: Velocity profiles for $n = 1.5$ at various values of time. (a) $t = 0.1$. (b) $t = 0.5$. (c) $t = 1$. (d) $t = 2$. (e) $t = 3$. (f) $t = 4$. (g) $t = 5$. (h) $t = 6$. (i) $t = 7$. (j) $t = 8$.

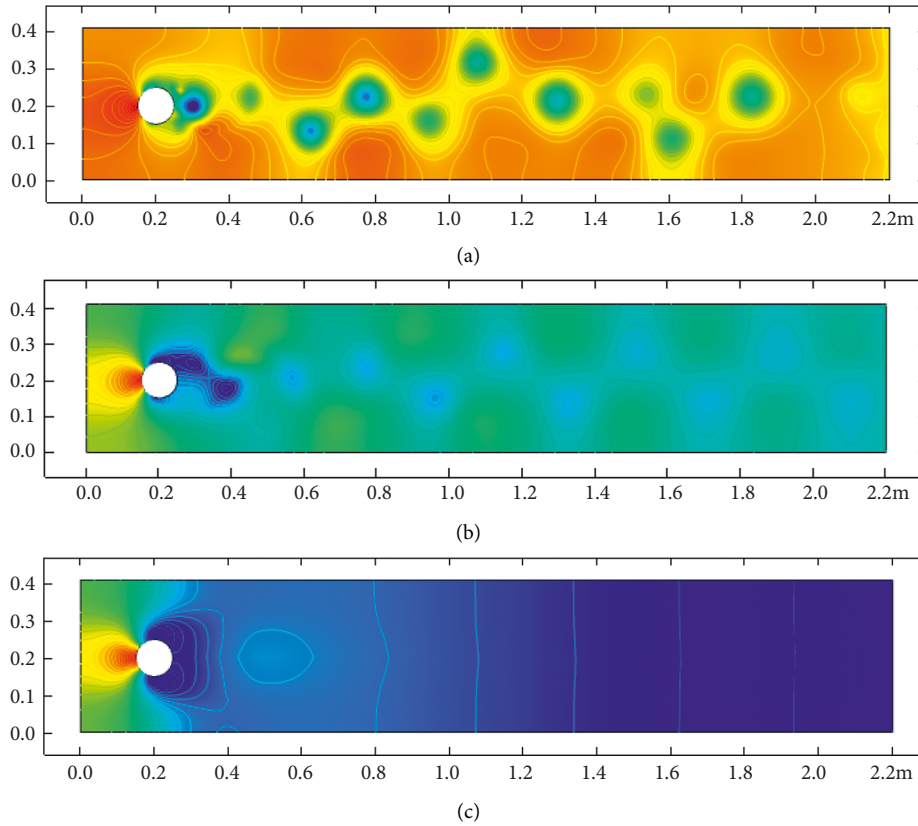


FIGURE 8: Pressure distribution in a channel for various n at $t = 8$. (a) $n = 0.5$, (b) $n = 1.0$, and (c) $n = 1.5$.

The incompressible generalized Navier–Stokes equations (1) and (2), as well as the rheological law (3), or power law, can be used to explain a variety of simulations. These equations help us understand the flow of materials in nature by describing particular transactions. We use finite element simulation for the numerical estimation of the governing equations because exact solutions to such problems are rare due to the model's high nonlinearity. The conforming element pair $\mathbb{P}_2 - \mathbb{P}_1$ is chosen for the velocity and pressure approximations in this direction. This element is a stable element pair [31–36] that meets the inf-sup

condition. The inner linear subproblems are solved using a direct solver, and discrete nonlinear algebraic systems are solved using Newton's method. The stopping criterion for the nonlinear iteration is set through a bound on the relative error as

$$\left| \frac{\aleph^{r+1} - \aleph^r}{\aleph^{r+1}} \right| < 10^{-6}, \quad (4)$$

where \aleph represents one of the component of solution (u, v, p) .

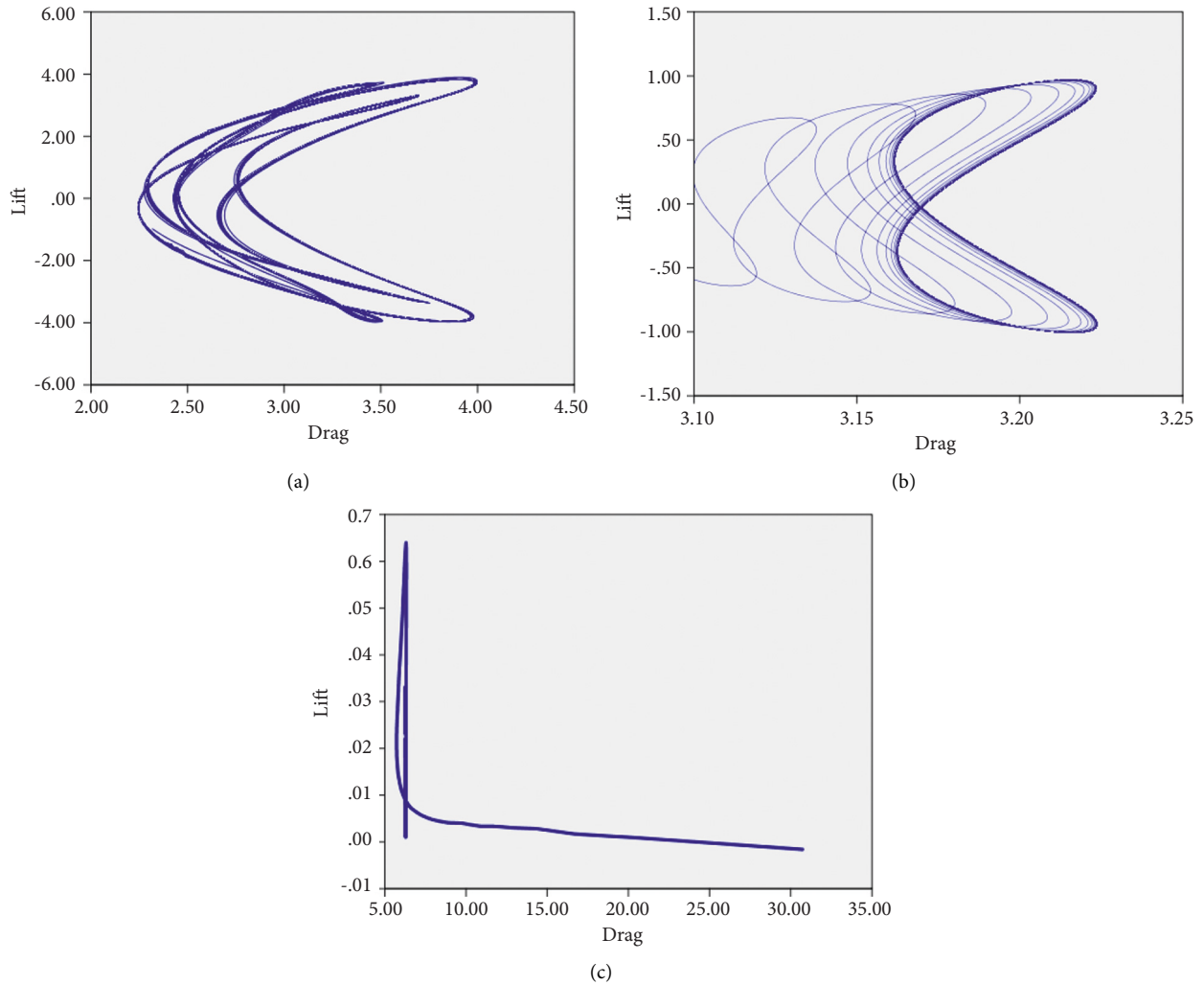


FIGURE 9: Phase-portrait (drag versus lift) (a) $n = 0.5$, (b) $n = 1.0$, and (c) $n = 1.5$.

3. Results and Discussions

The periodic flow of incompressible and unsteady power law fluids is numerically investigated by implementing the finite element method. For the validation of the code, we first simulate the case for $n = 1$, $Re = 100$ which corresponds to the Newtonian case for which the reference data is available in [8]. The viscosity of time-independent nonlinear fluids is only affected by shear rate and temperature. Shear-thinning, shear thickening, and plasticization viscosity increase with increased shear rate. The visual impact of drag and lift with respect to time can be seen in Figures 2–4 for all three cases of n . The considered time interval $0 < t \leq 10$ seconds is enough for hydrodynamic forces to get stable. Overall, there is not much variation in the amplitude of drag and lift from 5 seconds onwards. Lift coefficient appeared to be symmetric $C_L = 0$ on the horizontal axis for shear thinning ($n = 0.5$) and Newtonian case ($n = 1$). In the shear thinning case ($n = 0.5$), the drag oscillates between 2.3 and 4 (Figure 3), while the lift starts from zero and varies between -4 and $+4$. From Figure 4(a) and Figure 4(b) it is seen that both drag and lift coefficients converge to respective steady state

constant values for $n = 1.5$ due to enhanced viscosity in shear-thickening case. The lift forces are most potent in the upward trend, as indicated by the negative C_L . Even the obstacle is arranged as the lift coefficient is negative, resulting in a computational configuration like this.

The velocity profiles at various time steps for $n = 1$, 0.5 and 1.5 are presented in Figures 5–7, respectively. The corresponding pressure plots are shown in Figures 8(a)–8(c). In Figure 5, using $n = 1$, we provided the time dependent fluid with a parabolic profile having velocity $U_{max} = 1.5$. It can be seen that as the fluid strikes the circular cylinder, at $t = 0.1$ it starts bifurcating and approximately at $t = 3$ approach the outlet of the channel.

The outcome of the velocity profile for the shear thinning case is shared in Figure 6. The flow is fully developed approximately for $t \geq 3$. Figure 7 reports the velocity variations for shear thickening fluid. Here the flow is fully developed and vortex formation does not occur due to high viscosity. At $t = 8$, the pressure distribution for each case of n is offered in Figure 8.

The periodic flow at $Re = 100$ has its impact on drag and lift patterns, as shown in Figure 9 in terms of phase-plots. It

is observed that for the Newtonian case $n = 1$, there exists a single closed orbit after the steady state is achieved; however, there exist multiple periodic orbits for $n = 0.5$. The case of $n = 1.5$ is different where there is not any closed trajectory. Physically, the Reynolds number corresponds to a direct increase in the inertial forces capable of laminar flow for a fixed viscous fluid [37]; therefore, in future works, we would like to increase the Reynolds number to see its impact on C_D and C_L and on the Strouhal number elaborating the frequency of vortex shedding for shear thinning and thickening cases. [38, 39].

4. Conclusions

We have considered the two-dimensional transient flow of an incompressible power law fluid over a circular cylinder inside a channel. A static circular cylinder of diameter 0.1 m is used as an obstacle. The two-dimensional flow equations solved using the finite element method (FEM). Power law index n is considered for three particular values ($n = 0.5, 1.0$, and 1.5) at base Reynolds number $Re = 100$. For the time interval $0 \leq t \leq 10$ seconds, the behavior of velocity and pressure is observed. Moreover, the effects of shear rate on the drag-lift phase plot are also discussed. The diagram of drag-lift phase provides the precise information about the variations of C_D and C_L . From the phase plots, it is concluded that for the Newtonian case $n = 1$, there is only one closed orbit after the steady state is reached, while for $n = 0.5$, there are multiple periodic orbits. For the case of shear thickening $n = 1.5$, there is not any closed trajectory.

Data Availability

The data used to support the findings of this study are available from the corresponding author upon request.

Conflicts of Interest

The authors declare that they have no conflicts of interest.

Acknowledgments

The authors would like to express their gratitude to Deanship of Scientific Research at King Khalid University, Saudi Arabia, for providing funding research group under the research grant number R.G.P. 2/51/43.

References

- [1] S. Hussain, F. Schieweck, and S. Turek, "An efficient and stable finite element solver of higher order in space and time for nonstationary incompressible flow," *International Journal for Numerical Methods in Fluids*, vol. 73, no. 11, pp. 927–952, 2013.
- [2] R. P. Chhabra, A. A. Soares, and J. M. Ferreira, "Steady non-Newtonian flow past a circular cylinder: a numerical study," *Acta Mechanica*, vol. 172, no. 1–2, pp. 1–16, 2004.
- [3] A. Sojoudi and S. C. Saha, "Shear thinning and shear thickening non-Newtonian confined fluid flow over rotating cylinder," *American Journal of Fluid Dynamics*, vol. 2, no. 6, pp. 117–121, 2012.
- [4] R. Mahmood, N. Kousar, K. Usman, and A. Mehmood, "Finite element simulations for stationary Bingham fluid flow past a circular cylinder," *Journal of the Brazilian Society of Mechanical Sciences and Engineering*, vol. 40, no. 9, p. 459, 2018.
- [5] R. Mahmood, N. Kousar, K. U. Rehman, and M. Mohasan, "Lid driven flow field statistics: a non-conforming finite element Simulation," *Physica A: Statistical Mechanics and Its Applications*, vol. 528, Article ID 121198, 2019.
- [6] K. Ur Rehman, R. Mahmood, N. Kousar, S. Bilal, and I. Zehra, "On magnetized liquid stream statistics in grooved channel: a Finite element visualization," *Physica A: Statistical Mechanics and Its Applications*, vol. 535, p. 122463, 2019.
- [7] C. H. K. Williamson, "Vortex dynamics in the cylinder wake," *Annual Review of Fluid Mechanics*, vol. 28, no. 1, pp. 477–539, 1996.
- [8] M. Schäfer, S. Turek, F. Durst, E. Krause, and R. Rannacher, "Benchmark computations of laminar flow around a cylinder," in *Flow Simulation with High-Performance Computers II*, vol. 48, pp. 547–566, Vieweg, 1996.
- [9] P. Sivakumar, R. Prakash Bharti, and R. P. Chhabra, "Effect of power-law index on critical parameters for power-law flow across an unconfined circular cylinder," *Chemical Engineering Science*, vol. 61, no. 18, pp. 6035–6046, 2006.
- [10] V. K. Patnana, R. P. Bharti, and R. P. Chhabra, "Two-dimensional unsteady flow of power-law fluids over a cylinder," *Chemical Engineering Science*, vol. 64, no. 12, pp. 2978–2999, 2009.
- [11] D. J. Tritton, "Experiments on the flow past a circular cylinder at low Reynolds numbers," *Journal of Fluid Mechanics*, vol. 6, no. 4, pp. 547–567, 1959.
- [12] P. M. Coelho and F. T. Pinho, "Vortex shedding in cylinder flow of shear-thinning fluids," *Journal of Non-newtonian Fluid Mechanics*, vol. 110, no. 2–3, pp. 143–176, 2003.
- [13] A. K. Gupta, A. Sharma, R. P. Chhabra, and V. Eswaran, "Two-dimensional steady flow of a power-law fluid past a square cylinder in a plane channel: momentum and heat-transfer characteristics," *Industrial & Engineering Chemistry Research*, vol. 42, no. 22, pp. 5674–5686, 2003.
- [14] R. P. Bharti, R. P. Chhabra, V. Eswaran, and V. Eswaran, "A numerical study of the steady forced convection heat transfer from an unconfined circular cylinder," *Heat and Mass Transfer*, vol. 43, no. 7, pp. 639–648, 2007.
- [15] D. Canuto and K. Taira, "Two-dimensional compressible viscous flow around a circular cylinder," *Journal of Fluid Mechanics*, vol. 785, pp. 349–371, 2015.
- [16] N. Kanaris, D. Grigoriadis, and S. Kassinos, "Three-dimensional flow around a circular cylinder confined in a plane channel," *Physics of Fluids*, vol. 23, no. 6, p. 64106, 2011.
- [17] B. N. Rajani, A. Kandasamy, and S. Majumdar, "Numerical simulation of laminar flow past a circular cylinder," *Applied Mathematical Modelling*, vol. 33, no. 3, pp. 1228–1247, 2009.
- [18] D. L. Tokpavi, J. Pascal, M. Albert, and L. Jossic, "Experimental study of the very slow flow of a yield stress fluid around a circular cylinder," *Journal of Non-newtonian Fluid Mechanics*, vol. 164, no. 1–3, pp. 35–44, 2009.
- [19] S. Mossaz, J. Pascal, and M. Albert, "Criteria for the appearance of recirculating and non-stationary regimes behind a cylinder in a viscoplastic fluid," *Journal of Non-newtonian Fluid Mechanics*, vol. 165, no. 21–22, pp. 1525–1535, 2010.
- [20] A. Nejat, V. Abdollahi, and K. Vahidkhal, "Lattice Boltzmann simulation of non-Newtonian flows past confined cylinders," *Journal of Non-newtonian Fluid Mechanics*, vol. 166, no. 12–13, pp. 689–697, 2011.

- [21] S. J. D. D'Alessio and J. P. Pascal, "Steady flow of a power-law fluid past a cylinder," *Acta Mechanica*, vol. 117, no. 1-4, pp. 87-100, 1996.
- [22] M. J. Whitney and G. J. Rodin, "Force-velocity relationships for rigid bodies translating through unbounded shear-thinning power-law fluids," *International Journal of Non-linear Mechanics*, vol. 36, no. 6, pp. 947-953, 2001.
- [23] A. A. Soares, J. M. Ferreira, and R. P. Chhabra, "Flow and forced convection heat transfer in crossflow of non-Newtonian fluids over a circular cylinder," *Industrial & Engineering Chemistry Research*, vol. 44, no. 15, pp. 5815-5827, 2005.
- [24] D. Stojkovich, M. Breuer, and F. Durst, "Effect of high rotation rates on the laminar flow around a circular cylinder," *Physics of Fluids*, vol. 14, pp. 3160-3178, 2002.
- [25] O. Posdziech and R. Grundmann, "A systematic approach to the numerical calculation of fundamental quantities of the two-dimensional flow over a circular cylinder," *Journal of Fluids and Structures*, vol. 23, no. 3, pp. 479-499, 2007.
- [26] S. Sen, S. Mittal, and G. Biswas, "Steady separated flow past a circular cylinder at low Reynolds numbers," *Journal of Fluid Mechanics*, vol. 620, pp. 89-119, 2009.
- [27] O. A. Abegunrin, I. L. Animasaun, and N. Sandeep, "Insight into the boundary layer flow of non-Newtonian Eyring-Powell fluid due to catalytic surface reaction on an upper horizontal surface of a paraboloid of revolution," *Alexandria Engineering Journal*, vol. 57, no. 3, pp. 2051-2060, 2018.
- [28] R. Mahmood, S. Bilal, I. Khan, N. Kousar, A. H. Seikh, and El-S. M. Sharif, "A comprehensive finite element examination of Carreau Yasuda fluid model in a lid driven cavity and channel with obstacle by way of kinetic energy and drag and lift coefficient measurements," *Journal of Materials Research and Technology*, vol. 9, no. 2, pp. 1785-1800, 2020.
- [29] K. U. Rehman, M. Y. Malik, R. Mahmood, N. Kousar, and I. Zehra, "A potential alternative CFD simulation for steady Carreau-Bird law-based shear thickening model: Part-I," *Journal of the Brazilian Society of Mechanical Sciences and Engineering*, vol. 41, no. 4, p. 176, 2019.
- [30] F. Mebarek-Oudina, "Numerical modeling of the hydrodynamic stability in vertical annulus with heat source of different lengths," *Engineering Science and Technology, an International Journal*, vol. 20, no. 4, pp. 1324-1333, 2017.
- [31] A. H. Majeed, R. Mahmood, W. S. Abbasi, and K. Usman, "Numerical computation of MHD thermal flow of cross model over an elliptic cylinder: reduction of forces via thickness ratio," *Mathematical Problems in Engineering*, vol. 2021, pp. 1-13, Article ID 2550440, 2021.
- [32] S. Bilal, R. Mahmood, A. H. Majeed, I. Khan, and K. S. Nisar, "Finite element method visualization about heat transfer analysis of Newtonian material in triangular cavity with square cylinder," *Journal of Materials Research and Technology*, vol. 9, no. 3, pp. 4904-4918, 2020.
- [33] R. Mahmood, S. Bilal, A. H. Majeed, I. Khan, and E.-S. M. Sherif, "A comparative analysis of flow features of Newtonian and power law material: a New configuration," *Journal of Materials Research and Technology*, vol. 9, no. 2, pp. 1978-1987, 2020.
- [34] R. Mahmood, S. Bilal, A. H. Majeed, I. Khan, and K. S. Nisar, "Assessment of pseudo-plastic and dilatant materials flow in channel driven cavity: application of metallurgical processes," *Journal of Materials Research and Technology*, vol. 9, no. 3, pp. 3829-3837, 2020.
- [35] A. H. Majeed, F. Jarad, R. Mahmood, and I. Saddique, "Topological characteristics of obstacles and nonlinear rheological fluid flow in presence of insulated fins: a fluid force reduction study," *Mathematical Problems in Engineering*, vol. 2021, pp. 1-15, Article ID 9199512, 2021.
- [36] H. Ahmad, R. Mahmood, M. B. Hafeez, A. Hussain Majeed, S. Askar, and H. Shahzad, "Thermal visualization of Ostwald-de Waele liquid in wavy trapezoidal cavity: effect of undulation and amplitude," *Case Studies in Thermal Engineering*, vol. 29, Article ID 101698, 2021.
- [37] I. L. Animasaun, N. A. Shah, A. Wakif, B. Mahanthesh, R. Siviraj, and O. K. Koriko, *Ratio of Momentum Diffusivity to Thermal Diffusivity, Introduction, Meta-Analysis, and Scrutinization*, Chapman and Hall/CRC, New York, 2022.
- [38] R. P. Chhabra, A. A. Soares, and J. M. Ferreira, "Steady non-Newtonian flow past a circular cylinder: a numerical study," *Acta Mechanica*, vol. 172, no. 1-2, pp. 1-16, 2004.
- [39] A. A. Soares, J. M. Ferreira, and R. P. Chhabra, "Flow and forced convection heat transfer in crossflow of non-Newtonian fluids over a circular cylinder," *Industrial & Engineering Chemistry Research*, vol. 44, no. 15, pp. 5815-5827, 2005.